

ARTICLE

Received 29 Jul 2015 | Accepted 15 Mar 2016 | Published 25 Apr 2016

DOI: 10.1038/ncomms11324

OPEN

miRNA863-3p sequentially targets negative immune regulator *ARLPKs* and positive regulator *SERRATE* upon bacterial infection

Dongdong Niu^{1,2,*}, Yifan E. Lii^{2,*}, Padmanabhan Chellappan², Lei Lei³, Karl Peralta², Chunhao Jiang^{1,2}, Jianhua Guo¹, Gitta Coaker³ & Hailing Jin²

Plant small RNAs play important roles in gene regulation during pathogen infection. Here we show that miR863-3p is induced by the bacterial pathogen *Pseudomonas syringae* carrying various effectors. Early during infection, miR863-3p silences two negative regulators of plant defence, atypical receptor-like pseudokinase1 (*ARLPK1*) and *ARLPK2*, both lacking extracellular domains and kinase activity, through mRNA degradation to promote immunity. *ARLPK1* associates with, and may function through another negative immune regulator *ARLPK1*-interacting receptor-like kinase 1 (*AKIK1*), an active kinase with an extracellular domain. Later during infection, miR863-3p silences *SERRATE*, which is essential for miRNA accumulation and positively regulates defence, through translational inhibition. This results in decreased miR863-3p levels, thus forming a negative feedback loop to attenuate immune responses after successful defence. This is an example of a miRNA that sequentially targets both negative and positive regulators of immunity through two modes of action to fine-tune the timing and amplitude of defence responses.

¹Department of Plant Protection, Nanjing Agriculture University, Nanjing 210095, China. ²Department of Plant Pathology and Microbiology, Center for Plant Cell Biology and Institute for Integrative Genome Biology, University of California, Riverside, California 92521, USA. ³Department of Plant Pathology, University of California, Davis, California 95616, USA. * These authors contributed equally to this work. Correspondence and requests for materials should be addressed to H.J. (email: hailingj@ucr.edu).

During pathogen infection, plants undergo reprogramming and fine-tuning of gene expression to activate innate immune responses, and small RNAs (sRNAs) are important regulators in this process^{1–4}. As the first layer of defence, plant pattern-recognition receptors detect conserved pathogen features called pathogen-associated molecular patterns (PAMPs), leading to PAMP-triggered immunity (PTI)⁵. Some pathogens deliver effector proteins to attenuate PTI; however, in resistant hosts, Nod-like receptor (NLR) proteins recognize cognate effectors and activate effector-triggered immunity (ETI), which is more specific, robust and rapid than PTI. ETI is often characterized by the hypersensitive response (HR), a type of cell death, at the site of infection^{6,7}. One well-studied effector-NLR model in *Arabidopsis* is the effector AvrRpt2 from the bacterial pathogen *Pseudomonas syringae* pv. *tomato* (*Pst*) DC3000 and its cognate plant host NLR protein RPS2 (refs 8,9).

sRNAs are critical regulators of plant defence responses and pathogen virulence^{1–4,10}. These microRNAs (miRNAs) and short interfering RNAs (siRNAs) are processed by Dicer or Dicer-like (DCL) proteins and then incorporated into Argonaute (AGO) proteins to form RNA-induced silencing complex to target genes with full or partial complementary sequences. sRNAs can induce gene silencing by guiding post-transcriptional gene silencing via mRNA degradation or translational inhibition, or transcriptional inhibition via DNA methylation or chromatin modification¹¹. During infection with *Pst* DC3000 carrying the effector gene *avrRpt2*, the natural antisense transcript-associated siRNA natsiRNAATGB2 silences a gene with pentatricopeptide repeats, which acts as a negative regulator of ETI mediated by RPS2 (ref. 12). A long siRNA, AtlsiRNA, also induced by *Pst* (*avrRpt2*), silences the *AtRAP* gene (*Arabidopsis thaliana* RNA-binding domain abundant in apicomplexans), which has a negative role in defence¹³. miR393 contributes to PTI by targeting auxin signalling receptors upon elicitor flg22 treatment or after infection with virulent *Pst* DC3000 (ref. 14). The complementary strand of miR393 within the sRNA duplex, miR393*, regulates ETI during infection of *Pst* (*avrRpt2*) by targeting a protein trafficking gene *MEMB12* (Membrin 12) to promote the secretion of antimicrobial PR (pathogenesis-related) proteins¹⁵. miR160a enhances PAMP-induced callose deposition by targeting auxin response factors¹⁶. In addition to these examples of sRNAs that are induced by pathogen infection, some sRNAs are downregulated by infection. For example, miR398b, which targets a cytochrome c oxidase and two copper superoxide dismutases, and miR773, which targets a DNA methyltransferase, *MET2*, both negatively regulate PAMP-induced callose deposition, as well as PTI against *Pst* (EV) and *Pst* (Δ hrcC)¹⁶. Collectively, these studies highlight the importance of sRNAs that target critical plant genes involved in immune signalling. However, no sRNAs are reported to target genes with antagonistic roles in plant immunity or any other cellular processes.

We previously identified miRNAs and siRNAs that are differentially expressed on infection with various bacterial *Pst* strains¹⁷. One of these miRNAs, miR863-3p, was highly upregulated by the avirulent strain *Pst* (*avrRpt2*); thus, we hypothesized that this miRNA may play an important role in ETI, and sought to characterize its targets and their function. Here we show that miR863-3p targets the putative pseudokinases, atypical receptor-like pseudokinase 1 (*ARLPK1*) and *ARLPK2*, early on during infection to boost plant defence. *ARLPK1* interacts with *ARLPK1*-interacting receptor-like kinase (*AKIK1*), an active kinase that also negatively regulates defence. Later during infection, miR863-3p silences *SERRATE* (*SE*)—a protein important for miRNA processing and accumulation^{18–21} and for defence—to form a negative feedback loop to regulate the level of

miR863-3p. Attenuation of immune responses after successful defence is possibly to conserve host resources for growth and reproduction.

Results

miR863-3p is induced by infection with avirulent *Pst* strains. To identify miRNAs involved in regulating immune responses to bacterial infection, we previously profiled sRNAs from plants challenged with virulent and avirulent bacterial strains, *Pst* (EV) and *Pst* (*avrRpt2*), respectively¹⁷. We found that miR863-3p was highly upregulated during *Pst* (*avrRpt2*) infection. miR863-3p is a 21-nucleotide (nt) miRNA originating from the 3'-arm of the precursor miRNA (Supplementary Fig. 1a)²². Northern blot analysis confirmed that miR863-3p was induced by an avirulent strain *Pst* (*avrRpt2*), but not by the virulent strain *Pst* carrying an empty vector (EV), a strain that has a mutation in its type III secretion system—*Pst* (Δ hrcC), or mock solution (10 mM MgCl₂; Fig. 1a). miR863-3p levels are also upregulated by avirulent strains *Pst* (*avrRpm1*) and *Pst* (*avrRps4*), although to a lesser degree compared with *Pst* (*avrRpt2*) (Supplementary Fig. 1b). Interestingly, miR863-5p, the complementary strand of miR863-3p, was not induced by any of these *Pst* strains, and thus is not likely to be involved in defence against *Pst* (Fig. 1b).

Biogenesis of miRNAs depends on DCL1, which processes pri-miRNAs, and is aided by interacting RNA-binding proteins HYL1 and SE to promote accurate processing²⁰. Northern blot analysis revealed that miR863-3p accumulation is dependent on DCL1 and SE, but independent of RDR6, which is involved in the biogenesis and amplification of siRNAs (Fig. 1c)¹¹. These results indicate that miR863-3p is indeed a true miRNA instead of a siRNA. Taken together, our results show that miR863-3p is dependent on DCL1 and SE, and it is induced by challenge with avirulent *Pst* strains, especially *Pst* (*avrRpt2*). Its complementary strand was not detected in our experiments, showing that miR863-3p is the stable miRNA strand during pathogen infection.

miR863-3p targets two ARLPKs and SE. We hypothesized that miR863-3p targets genes involved in immune responses, but since miR863-3p has no validated targets in existing databases, we predicted its potential targets (Methods). miR863-3p potentially targets the coding sequences of two atypical receptor-like kinases (RLKs), *ARLPK1* and *ARLPK2*, belonging to the leucine-rich repeat (LRR) III RLK subfamily²³, as well as the 3'-untranslated region (UTR) of *SE*, which encodes a zinc-finger protein found in both the miRNA biogenesis DCL1 complex¹⁹, and the nuclear cap-binding protein complex²⁴ (Fig. 2a). Typical RLKs have an extracellular ligand-binding domain, a single transmembrane region and an intracellular kinase domain²³. Both *ARLPK1* and *ARLPK2* have a signal peptide sequence overlapping with their N-terminal transmembrane domain (Supplementary Fig. 2a,b) and lack extracellular domains²³. They also have variations in the conserved features of functional kinase domains such as the glycine-rich loop, VAIK motif and HRD motif (Supplementary Fig. 3), and are thus predicted pseudokinases²⁵. Because *ARLPK1* and *ARLPK2* are missing conserved key residues in the consensus motifs and are lacking extracellular domains, we named them atypical receptor-like pseudokinases (*ARLPK1*, At5g61570; and *ARLPK2* At5g07620). miR863-3p is also predicted to target a third gene *SE*, which is involved in the accumulation of miRNAs, including miR863-3p (Fig. 1c). During *Pst* (*avrRpt2*) infection, the mRNA levels of the two *ARLPKs* are downregulated compared with mock-infected plants; however, *SE* mRNA levels are upregulated. In contrast, the levels of all three transcripts do

not change significantly during *Pst* (EV) or *Pst* ($\Delta hrcC$) infection (Fig. 2b).

To confirm that *ARLPK1* and *ARLPK2* are true targets of miR863-3p, we performed *Agrobacterium*-mediated transient co-expression assays in *Nicotiana benthamiana* using wild-type (wt) and mutated (m) kinase genes. The mutated kinases have an altered miR863-3p target site, yet the predicted amino-acid sequence is unchanged (Fig. 2a). MIR863 co-expression with wtARLPK1 or wtARLPK2 resulted in a decrease of the mRNA levels of both kinases, while co-expression with mARLPK1 or mARLPK2 did not affect the mRNA levels of mARLPK1 or mARLPK2 (Fig. 2c). In addition, we performed RNA-ligase mediated 5' rapid amplification of cDNA ends (RLM-RACE) in *Pst* (*avrRpt2*)-infected *Arabidopsis* to map miR863-3p-guided cleavage sites in *ARLPK* mRNA. As expected, the majority of the 5'-RACE cloned products mapped to the predicted target site in *ARLPK1* and *ARLPK2* mRNAs (Fig. 2d). These data indicate *ARLPK1* and *ARLPK2* are direct targets of miR863-3p, and they are silenced via mRNA cleavage and degradation.

In plants, most miRNAs silence their targets by directing mRNA cleavage and degradation, while others mediate translational inhibition²⁶. In mammals, most miRNA target sites for translational inhibition are located in the 3'-UTR, and the target site of miR863-3p in *SE* is also at the beginning of the 3'-UTR. *SE* mRNA levels are not downregulated by miR863-3p (Fig. 2b), even though the nucleotide alignment shows very few mismatches (Fig. 2a). Thus, it is possible that miR863-3p silences *SE* through translational inhibition. In mammals, target mRNAs silenced by RNA-induced silencing complex via translational repression are delivered to and accumulate in processing (P)-bodies²⁷. Thus, it is possible that we see elevated *SE* transcripts not only because of continual transcription of *SE* due to the absence of *SE* protein product but also because of the accumulation of sequestered *SE* mRNAs in P-bodies. To test

that hypothesis, we generated constructs of green fluorescent protein (GFP) fused to a wt version of truncated *SE* that includes only the 3'-UTR (GFP-wtSE-3'-UTR) or a mutated truncated version of *SE* with an altered miRNA target site (GFP-mSE-3'-UTR; Fig. 2a). We co-expressed the fusions with MIR863 in *N. benthamiana*, and western blotting revealed that GFP-wtSE-3'-UTR, but not GFP-mSE-3'-UTR, levels were downregulated (Fig. 2e). To confirm this result *in vivo*, we obtained an anti-*SE* antibody and detected *SE* protein levels in *Arabidopsis* plants challenged with *Pst* strains. Western blot analysis revealed that *SE* protein levels are downregulated by *Pst* (*avrRpt2*) but not by *Pst* ($\Delta hrcC$) or *Pst* (EV) (Fig. 2f). These results suggest that miR863-3p targets and silences *SE* by inhibiting its translation. Thus, miR863-3p uses two different modes of action to silence its targets—it suppresses the two *ARLPKs* via mRNA cleavage and degradation and inhibits *SE* by translational inhibition.

ARLPKs are negative regulators of disease resistance.

To investigate the role of miR863-3p during plant immune responses, we created transgenic plants overexpressing MIR863 under the control of the cauliflower mosaic virus 35S promoter. Figure 3a shows nine such overexpression (OE) lines. The lines with very high miR863-3p expression (such as MIR863-OE1 and -OE2 lines) resembled the *serrate* mutant phenotype²⁸, further supporting that *SE* is indeed a miR863-3p target (Fig. 3b). Only a slight increase of miR863-3p was observed after infection with *Pst* (*avrRpt2*) in the OE lines, most likely because miR863-3p levels are already very high (Supplementary Fig. 4). We also detected very low levels of miR863-5p in some of the OE lines (Fig. 3a). We chose two transgenic lines with high miR863-3p levels, MIR863-OE1 and -OE2, and one with lower levels, MIR863-OE3, for functional analyses (Fig. 3a). MIR863-OE1 and -OE2 plants were slightly smaller than Col-0 WT plants (Fig. 3b, upper

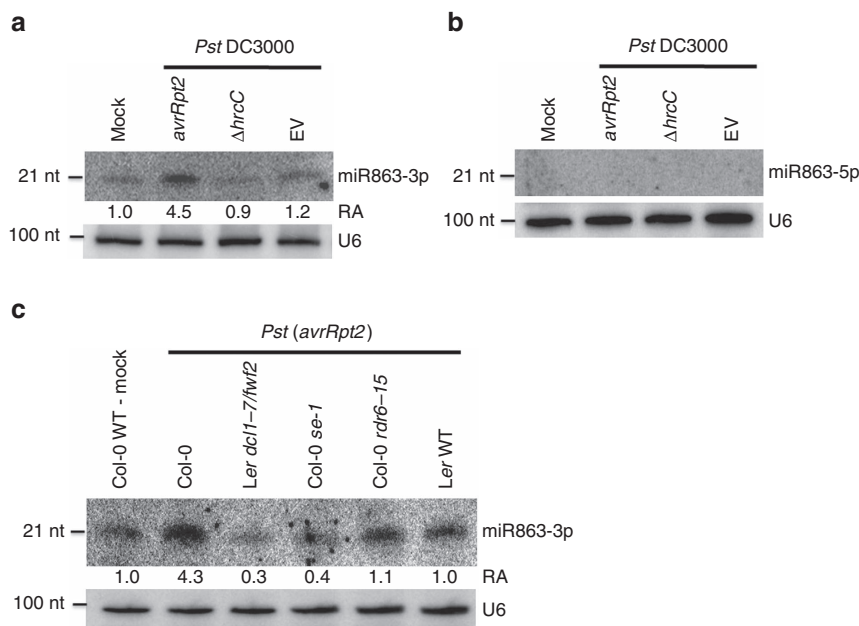


Figure 1 | miR863-3p is induced by *Pst* carrying the effector *avrRpt2*. (a) miR863-3p and (b) miR863-5p levels in mock-, *Pst* (*avrRpt2*)-, *Pst* ($\Delta hrcC$)- and *Pst* (EV)-infected Col-0 WT plants were detected by northern blot analysis. Bacterial inoculum concentration: 1×10^7 c.f.u. per ml. Leaf tissue was collected at 14 h.p.i. U6 was used as a loading control. Relative abundance (RA) levels are indicated. Similar results were obtained from three biological replicates. (c) miR863-3p levels in various *Pst* (*avrRpt2*)-infected mutants defective in miRNA biogenesis (*Ler dcl1-7/fwf2* and *Col-0 se-1*) or siRNA biogenesis (*Col-0 rdr6-15*) are detected by northern blot analysis. Mock-treated and *Pst* (*avrRpt2*)-infected Col-0 WT and *Pst* (*avrRpt2*)-infected *Ler WT* were used as controls. Bacterial inoculum concentration: 1×10^7 c.f.u. per ml. Leaf tissue was collected at 14 h.p.i. U6 was used as a loading control. RA levels are indicated. Similar results were obtained from three biological replicates.

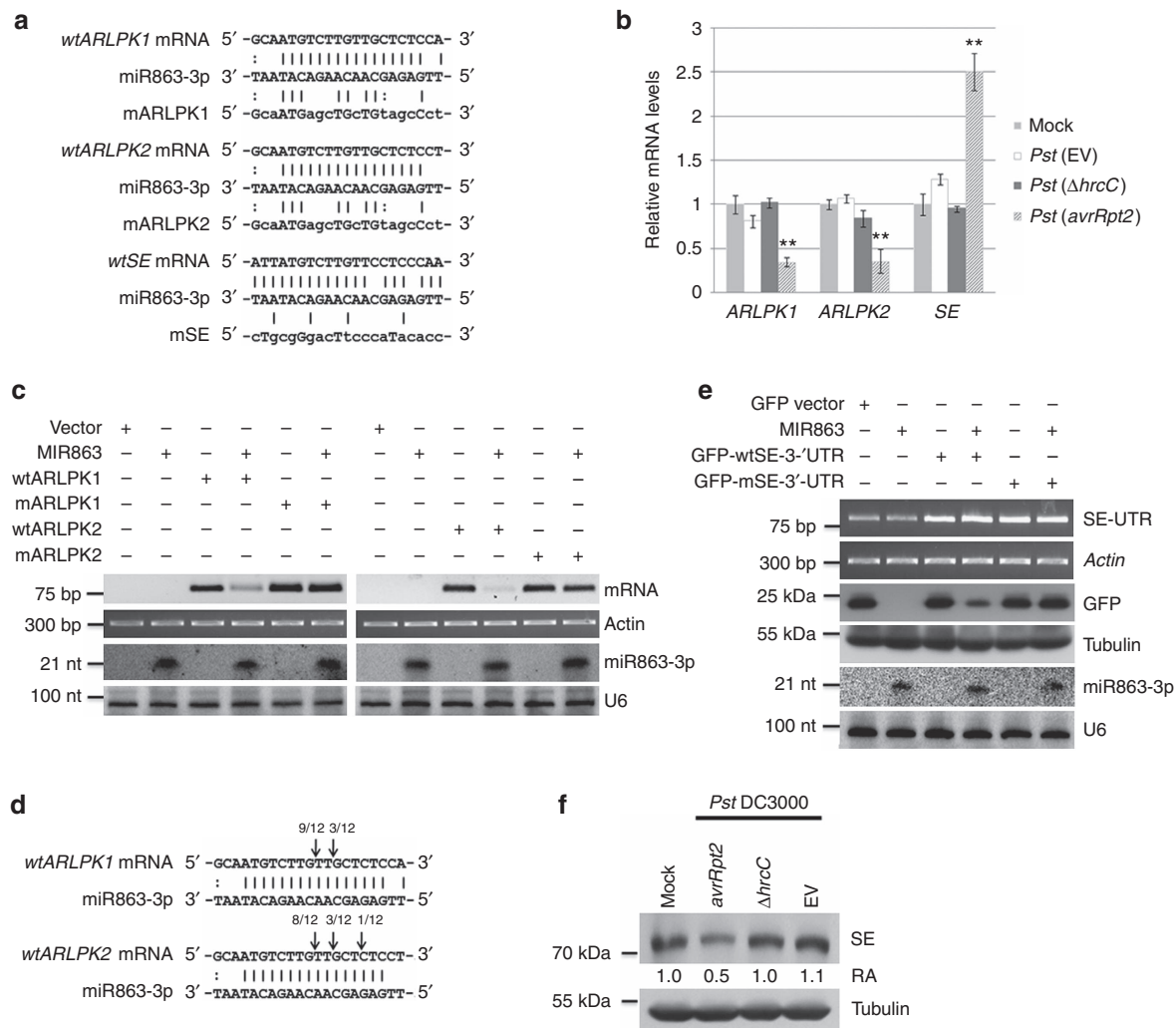


Figure 2 | miR863-3p targets and silences *ARLPK1* and *ARLPK2* and *SE* by two modes of action. (a) Nucleotide sequences of wt and mutated (m) versions of *ARLPK1*, *ARLPK2* and *SE* aligned against the miR863-3p sequence. (b) Relative expression levels of *ARLPK1*, *ARLPK2* and *SE* transcripts in mock- and *Pst* (EV), *Pst* ($\Delta hrcC$) and *Pst* (*avrRpt2*)-infected Col-0 WT plants were detected by real-time RT-PCR. Bacterial inoculum concentration: 1×10^7 c.f.u. per ml. Leaf tissue was collected 14 h.p.i. Relative mRNA levels in mock-infected plants were set at 1. Error bars indicate s.d. from three technical replicates. Similar results were obtained from three biological replicates. ***P* value < 0.01 (Student's *t*-test). (c) *Agrobacterium*-mediated transient co-expression assay with WT (wtARLPK1 and wtARLPK2) or mutated kinases (mARLPK1 and mARLPK2) and MIR863. mRNA levels of the wt and mutant kinases were detected by RT-PCR. rRNA was used as a loading control. miR863-3p levels were detected by northern blot analysis. U6 was used as a loading control. Similar results were obtained from two biological replicates. (d) Cleavage sites of *ARLPK1* and *ARLPK2* mRNAs were revealed by mapping cloned RLM-5'-RACE products using *Pst* (*avrRpt2*)-infected WT *Arabidopsis* plants. Arrows indicate positions and proportions of clones mapping to the sites. (e) *Agrobacterium*-mediated transient co-expression assay with GFP-tagged wt (GFP-wtSE-3'-UTR) or mutated (GFP-mSE-3'-UTR) 3'-UTR SE fragment and MIR863. wtSE-GFP and mSE-GFP mRNA were detected by RT-PCR using primers specific to the SE 3'-UTR. Actin was used as a loading control. GFP protein levels were detected by western blot. α -Tubulin was used as a loading control. miR863-3p levels were detected by northern blot analysis. U6 was used as a loading control. Similar results were obtained from two biological replicates. (f) SE protein levels in mock-, *Pst* (*avrRpt2*)-, *Pst* ($\Delta hrcC$)- and *Pst* (EV)-infected Col-0 WT plants were detected by western blot using an anti-SE antibody. Bacterial inoculum concentration: 1×10^7 c.f.u. per ml. Leaf tissue was collected at 14 h.p.i. α -Tubulin was used as a loading control. Relative abundance (RA) levels are indicated. Similar results were obtained from two biological replicates.

panels). In the MIR863 overexpression lines, *ARLPK1* and *ARLPK2* mRNA levels are downregulated while *SE* mRNA levels are elevated, as shown by real-time reverse transcription-PCR (RT-PCR) results (Fig. 3c). *SE* mRNA levels are elevated just as in *Pst* (*avrRpt2*)-infected plants (Fig. 2a), most likely due to feedback compensation to increase transcription and also sequestering of transcripts in P-bodies²⁷. *SE* protein levels in the overexpression lines are significantly lower compared with Col-0 WT, especially in MIR863-OE1 and -OE2 (Fig. 3d). Interestingly, even though the target genes were downregulated, the MIR863 overexpression lines showed no altered disease

resistance to *Pst* (EV) or *Pst* (*avrRpt2*) compared with Col-0 WT plants (Fig. 3e).

To understand why overexpressing MIR863 did not have an effect on the defence response, we decided to study the function of miR863-3p targets individually. First, we focused on the functional analysis of the two ARLPKs and obtained the null mutants SALK_144635 (*arlpk1-1*) and SALK_040744C (*arlpk2-1*)²⁹. Each mutant contains a T-DNA insertion in the first exon (Supplementary Fig. 5a), as confirmed by RT-PCR (Supplementary Fig. 5b). The single mutants were developmentally similar to Col-0 WT plants (Supplementary

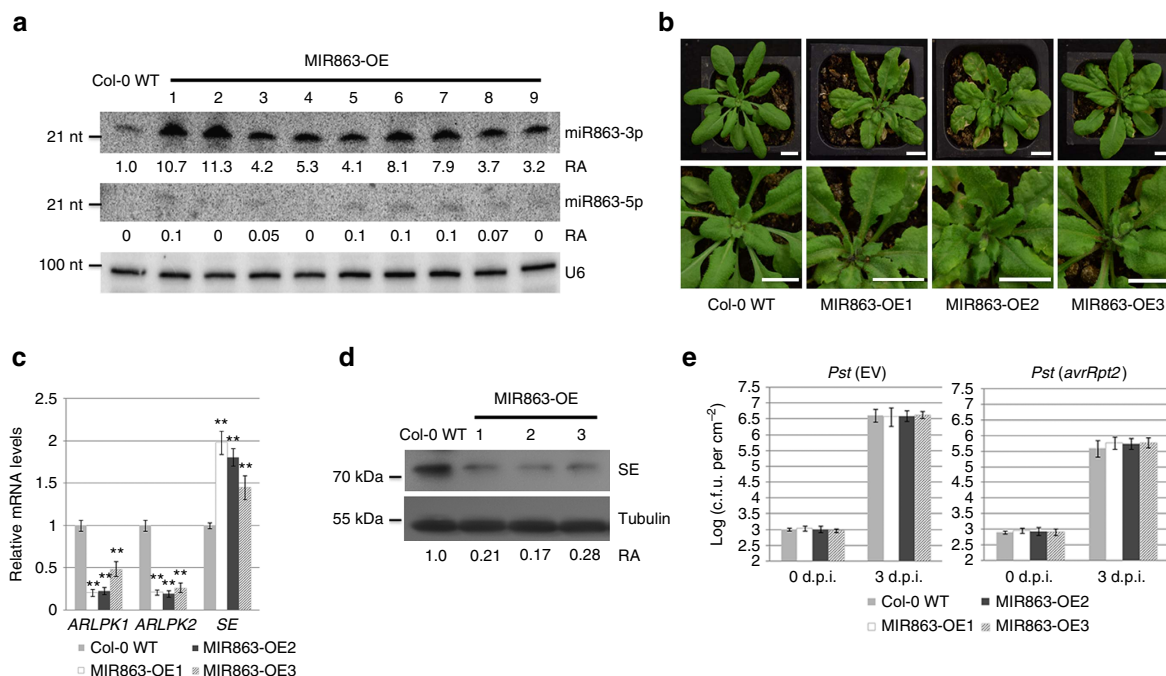


Figure 3 | Plants overexpressing MIR863 show serrate leaves and have downregulated ARLPK1 and ARLPK2 mRNA and SE protein levels.

(a) miRNA863-3p and miRNA863-5p levels were detected in Col-0 WT and MIR863-OE lines #1–9. U6 was used as a loading control. Relative abundance (RA) levels are indicated. miRNA863-5p RA levels were measured compared with the miRNA863-3p levels in Col-0 WT. Similar results were obtained from two biological replicates. (b) Phenotypes of 4-week-old MIR863 OE plants. Out of the 20 lines tested, 4 highly expressed lines resembled the *serrate* mutant phenotype (MIR863-OE1 and -OE2 are shown), while 7 medium expressed lines showed a weak serrated leaf phenotype (MIR863-OE3 is shown). Scale bar, 10 mm. (c) ARLPK1, ARLPK2 and SE transcript levels in Col-0 WT and MIR863-OE plants were detected by real-time RT-PCR. Error bars indicate s.d. from three technical replicates. Similar results were obtained from three biological replicates. ***P* value < 0.01 (Student's *t*-test). (d) SE protein levels were detected in *Pst* (*avrRpt2*)-infected Col-0 WT and MIR863-OE plants by western blot analysis using an anti-SE antibody. Bacterial inoculum concentration: 1×10^7 c.f.u. per ml. Leaf tissue was collected at 14 h.p.i. α -Tubulin was used as a loading control. RA levels are indicated. Similar results were obtained from two biological replicates. (e) Bacterial growth in *Pst* (EV)- and *Pst* (*avrRpt2*)-infected Col-0 WT and MIR863-OE plants. Bacterial inoculum concentration: 5×10^5 c.f.u. per ml. Bacterial growth was measured at 3 d.p.i. Error bars represent s.d. for at least 15 leaf discs. Similar results were obtained from three biological replicates.

Fig. 5c) and did not differ from Col-0 WT in defence response to infection with *Pst* (EV) or *Pst* (*avrRpt2*) (Supplementary Fig. 5d). This lack of disease phenotype may be due to functional redundancy, so we generated the *arlpk1-1 arlpk2-1* double mutant. The *arlpk1-1 arlpk2-1* plants were smaller compared with Col-0 WT (Fig. 4a), and when infected with *Pst* (EV) and *Pst* (*avrRpt2*), *arlpk1-1 arlpk2-1* plants exhibited less bacterial growth in both cases (Fig. 4b). To confirm the phenotype of enhanced resistance in the double mutant, we measured the expression of antimicrobial pathogenesis-related protein, PR1, a marker for salicylic acid-dependent disease responses. At 12 h post inoculation (h.p.i.), *arlpk1-1 arlpk2-1* showed higher PR1 protein expression compared with Col-0 WT after infection with *Pst* (EV) and *Pst* (*avrRpt2*) (Fig. 4c), indicating that ARLPK1 and ARLPK2 are functionally redundant and negatively regulate plant immune responses.

We furthermore generated transgenic *Arabidopsis* overexpressing ARLPK1 with a mutation in the miR863-target site (mARLPK1-OE, as in Fig. 2a) in the Col-0 WT background. We selected two overexpression lines, mARLPK1-OE1 and -OE2, exhibiting high ARLPK1 transcript levels as detected by real-time RT-PCR for further functional analysis (Fig. 4d). Both lines are more susceptible to *Pst* (EV) and *Pst* (*avrRpt2*) compared with Col-0 WT, further supporting that ARLPKs are negative regulators of plant immunity (Fig. 4e). miR863-3p-mediated silencing of ARLPK1 during bacterial infection is important to promote plant defence responses.

ARLPKs are putative pseudokinases. As noted above, ARLPK1 and ARLPK2 have variations in the conserved motifs of functional kinase domains such as the glycine-rich loop (GXGXXG), VAIK motif and HRD motif (Supplementary Fig. 3), and are thus predicted pseudokinases. The glycine loop is located in subdomain I near the catalytic domain and is found in many nucleotide-binding proteins as well as in protein kinases²⁵. Both ARLPK1 and ARLPK2 have a serine substitution for the second glycine in the loop. The VAIK, HRD and DFG motifs are all found in the catalytic domain. The lysine in the VAIK motif in subdomain II interacts with ATP²⁵. ARLPK1 and ARLPK2 have a VRVL and an IRVL motif, respectively, and are thus missing the lysine residue; it has not been demonstrated that these motifs can bind ATP. The aspartic acid in the HRD motif in subdomain IV is the base acceptor for proton transfer²⁵. However, both pseudokinases have a HGN motif containing an uncharged asparagine. Finally, the aspartic acid in the DFG motif, which is found in catalytic domains and binds Mg^{2+} ions that coordinate the phosphates of ATP in the ATP-binding cleft²⁵, is conserved in ARLPK1 and ARLPK2 (Supplementary Fig. 3). As predicted, we were unable to detect autophosphorylation *in vitro* using recombinant ARLPK1 and ARLPK2 proteins (Fig. 4f). In contrast, we were able to clearly detect kinase activity for the RPM1-induced protein kinase (RIPK), which was used as a positive control³⁰. These data support that ARLPK1 and ARLPK2 are most likely pseudokinases.

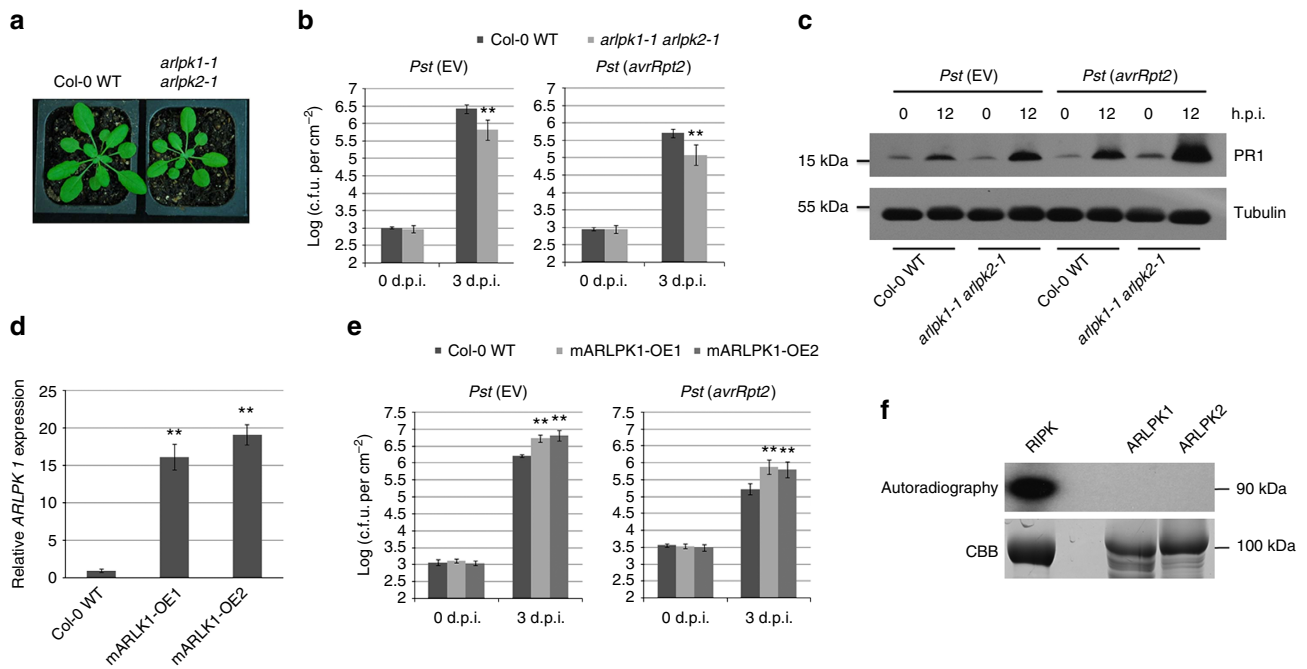


Figure 4 | Analysis of the *arlpk1-1 arlpk2-1* double mutant. (a) Phenotype of 4-week-old *arlpk1-1 arlpk2-1* double mutants compared with Col-0 WT plants. (b) Bacterial growth in *Pst* (EV)- and *Pst* (*avrRpt2*)-infected Col-0 WT and *arlpk1-1 arlpk2-1* double mutants. Bacterial inoculum concentration: 5×10^5 c.f.u. per ml. Bacterial growth was measured at 3 d.p.i. Error bars represent s.d. for at least 15 leaf discs. Similar results were obtained in three biological replicates. ***P* value < 0.01 (Student's *t*-test). (c) PR1 protein levels were detected in *Pst* (EV)- and *Pst* (*avrRpt2*)-infected Col-0 WT and *arlpk1-1 arlpk2-1* double mutants by western blot using an anti-PR1 antibody. Bacterial inoculum concentration: 1×10^7 c.f.u. per ml. Samples were collected at 0 and 12 h.p.i. α -Tubulin was used as a loading control. Similar results were obtained from two biological replicates. (d) Levels of ARLPK1 transcript in Col-0 WT, mARLPK1-OE1 and mARLPK1-OE2 lines were detected by real-time RT-PCR. Error bars indicate s.d. from three technical replicates. Similar results were obtained in three biological replicates. ***P* value < 0.01 (Student's *t*-test). (e) Bacterial growth in *Pst* (EV)- and *Pst* (*avrRpt2*)-infected Col-0 WT and mARLPK1-OE plants. Bacterial inoculum concentration: 5×10^5 c.f.u. per ml. Bacterial growth was measured 3 d.p.i. Error bars represent s.d. for at least 15 leaf discs. Similar results were obtained from three biological replicates. ***P* value < 0.01 (Student's *t*-test). (f) Recombinant MBP-tagged kinase domains of RIPK, ARLPK1 and ARLPK2 proteins were subjected to a radioactive kinase assay and kinase activity was detected using autoradiography. Bottom panel: SDS-PAGE gel stained with coomassie brilliant blue (CBB) demonstrating protein abundance. Similar results were obtained from two biological replicates.

ARLPK1 interacts with AKIK1 to regulate plant immunity.

Both ARLPKs have a predicted transmembrane domain, so we determined their subcellular localization in *N. benthamiana* with confocal microscopy. However, the endoplasmic reticulum (ER) signal peptide in ARLPK1 and ARLPK2 overlaps with the predicted transmembrane domain (Supplementary Fig. 2). We originally thought that the pseudokinases would be localized in the plasma membrane (PM) and we used a PM-localized protein RLK (At5g23740)-cyan fluorescent protein (CFP) as control. To our surprise, we found that both ARLPK1-yellow fluorescent protein (YFP) and ARLPK2-YFP predominantly localize in the ER (Supplementary Fig. 6). We confirmed this using a mCherry-tagged ER organelle marker³¹ (ER-mCherry) as a control. ARLPK1-YFP and ARLPK2-YFP overlapped with ER-mCherry in merged images, and Hechtian strands were not visible after plasmolysis treatment (Fig. 5a, upper panels). These results only show the steady-state localization of these fluorescently tagged proteins. Trafficking or movement of some RLKs during pathogen challenge is often observed, as in the case of FLS2, which undergoes endocytosis upon flg22 treatment³². We also checked the localization of ARLPKs after *Pst* (*avrRpt2*) challenge; however, we did not see any changes in the localization after *Pst* (*avrRpt2*) infection, both with and without plasmolysis treatment (Fig. 5a, lower panels).

Because these two kinases are putative pseudokinases that lack an extracellular domain, we hypothesized that ARLPK1 and ARLPK2 function with another RLK to perceive and/or regulate extracellular signals. We searched for interacting proteins on the

Arabidopsis Interactions Viewer³³ (<http://bar.utoronto.ca/>), and found AT5G59650, a LRR I subfamily RLK, which may interact with ARLPK1. Thus, we named it AKIK1. Owing to non-complementarity in the nucleotide alignment, AKIK1 is not likely to be targeted by miR863-3p. AKIK1 contains a malectin domain and two LRR domains in its predicted extracellular region (Supplementary Fig. 7a,b). We found that AKIK1-CFP also predominantly localizes in the ER in untreated and pathogen-treated plants, both with and without plasmolysis treatment, as seen in the merged image with ER-mCherry (Fig. 5b, left panels), and it also co-localizes with ARLPK1-YFP (Fig. 5b, right panels).

We confirmed by co-immunoprecipitation (Co-IP) that ARLPK1, but not ARLPK2, interacts with AKIK1 (Fig. 6a). We hypothesized that due to its association with ARLPK1, AKIK1 also has a role in plant defence. We obtained two T-DNA insertion mutant lines, *akik1-1* (SALK_022711C) and *akik1-2* (CS848612), which have T-DNA insertions in the fourth and ninth introns of AKIK1, respectively (Supplementary Fig. 8a). These two lines are both null mutants of AKIK1, as confirmed by RT-PCR (Supplementary Fig. 8b), and neither had any obvious developmental phenotypes compared with Col-0 WT (Supplementary Fig. 8c). Both *akik1-1* and *akik1-2* were more resistant to infection with *Pst* (EV) and *Pst* (*avrRpt2*) compared with Col-0 WT plants (Fig. 6b). Because both mutants showed the same disease phenotypes, we used *akik1-1* for further analysis. In agreement with the bacterial growth assays, PR1 protein levels were higher in *akik1-1* compared with Col-0 WT 12 h.p.i. with *Pst* (EV) and *Pst* (*avrRpt2*), although to a lesser extent with *Pst* (EV)

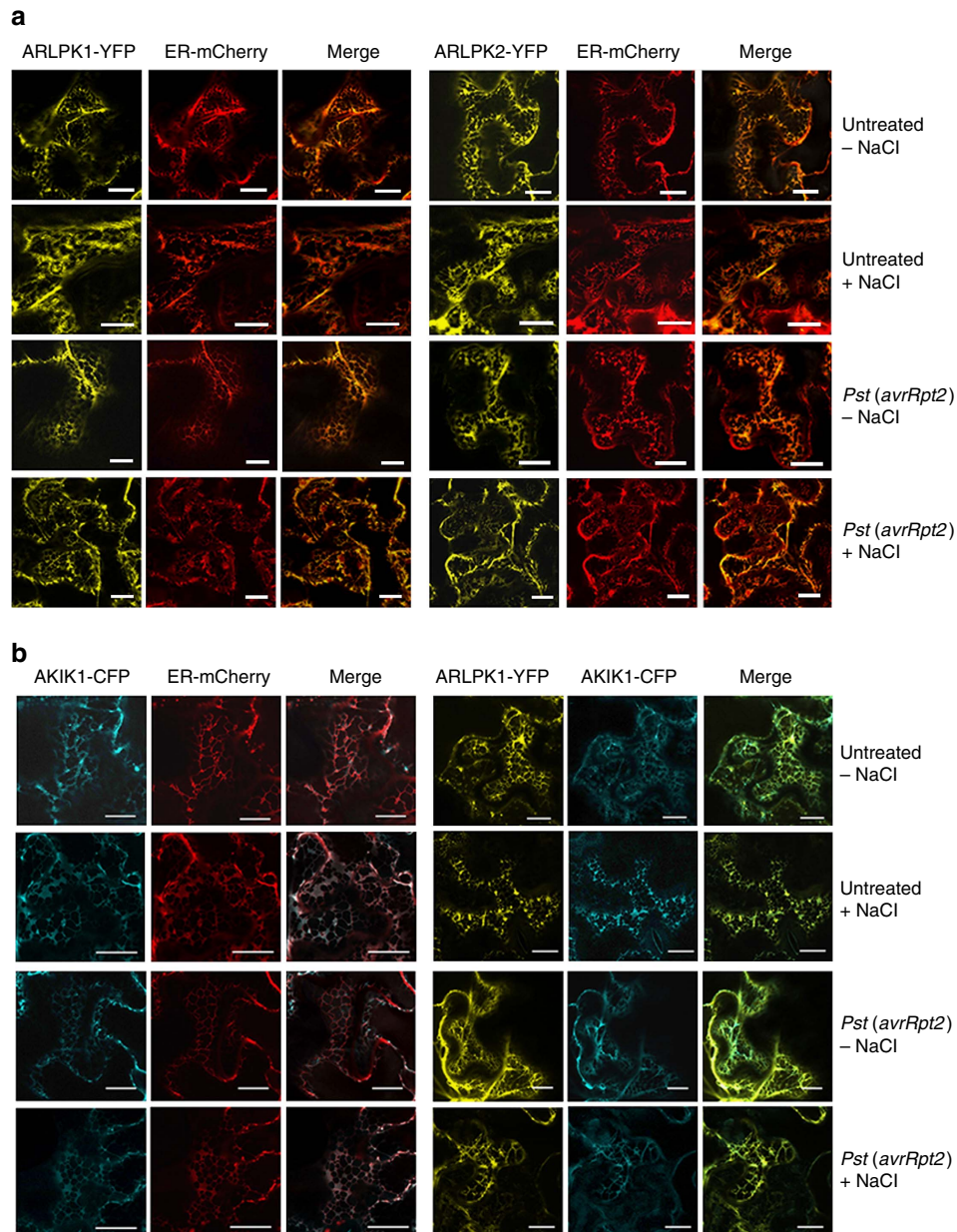


Figure 5 | ARLPKs and AKIK1 predominantly localize in the ER. (a) Co-localization of ARLPK1-YFP or ARLPK2-YFP with ER-mCherry in *N. benthamiana* was observed with confocal microscopy. Untreated plants were visualized 60 h after co-infiltration. Treated plants were infected 48 h after co-infiltration with *Pst (avrRpt2)* and visualized 12 h.p.i. Bacterial inoculum concentration: 1×10^7 c.f.u. per ml. Fluorescent images of the middle of the cell were taken separately then merged. Samples were visualized without (– NaCl) and with (+ NaCl) plasmolysis treatment (5% NaCl for 5–10 min). Scale bars, 20 μ m. **(b)** Co-localization of AKIK1-CFP with ER-mCherry and ARLPK1-YFP with AKIK1-CFP in *N. benthamiana* was observed with confocal microscopy. Untreated plants were visualized 60 h after co-infiltration. Treated plants were infected 48 h after co-infiltration with *Pst (avrRpt2)* and visualized 12 h.p.i. Tissue was collected for imaging 12 h.p.i. Bacterial inoculum concentration: 1×10^7 c.f.u. per ml. Fluorescent images of the middle of the cell were taken separately then merged. Samples were visualized without (– NaCl) and with (+ NaCl) plasmolysis treatment (5% NaCl for 5–10 min). Scale bars, 20 μ m.

(Fig. 6c). To confirm the roles of ARLPK1, ARLPK2 and AKIK1 in PTI, we performed assays that measured PAMP responses to flg22 treatment. We measured PTI-responsive gene flg22-induced receptor-like kinase 1 (*FRK1*) by real-time RT-PCR after treatment with flg22. In agreement with the bacterial growth assay results, the double mutant *arlpk1-1 arlpk2-1* and the *akik1-1* mutant showed highly increased *FRK1* expression compared with Col-0 WT (Fig. 6d). Mitogen-activated protein kinase 3 (MPK3) and MPK6 are two kinases involved in the MAP kinase signalling cascade, which act downstream of FLS2 to confer disease resistance³⁴. The *arlpk1-1 arlpk2-1* double mutant and the

akik1-1 mutant showed significantly higher MPK3 and MPK6 levels compared with Col-0 WT after flg22 treatment (Fig. 6e). Unlike ARLPK1 and ARLPK2, AKIK1 does possess conserved catalytic residues in its kinase domain (Supplementary Fig. 3). The kinase domain of AKIK1 was expressed and purified from *Escherichia coli* and subjected to an *in vitro* radiolabelled kinase assay. Consistent with its conserved catalytic residues, we were able to detect autophosphorylation activity for AKIK1, demonstrating that it is an active kinase (Fig. 6f). Taken together, the results show ARLPK1, ARLPK2 and AKIK1 all negatively regulate ETI and PTI.

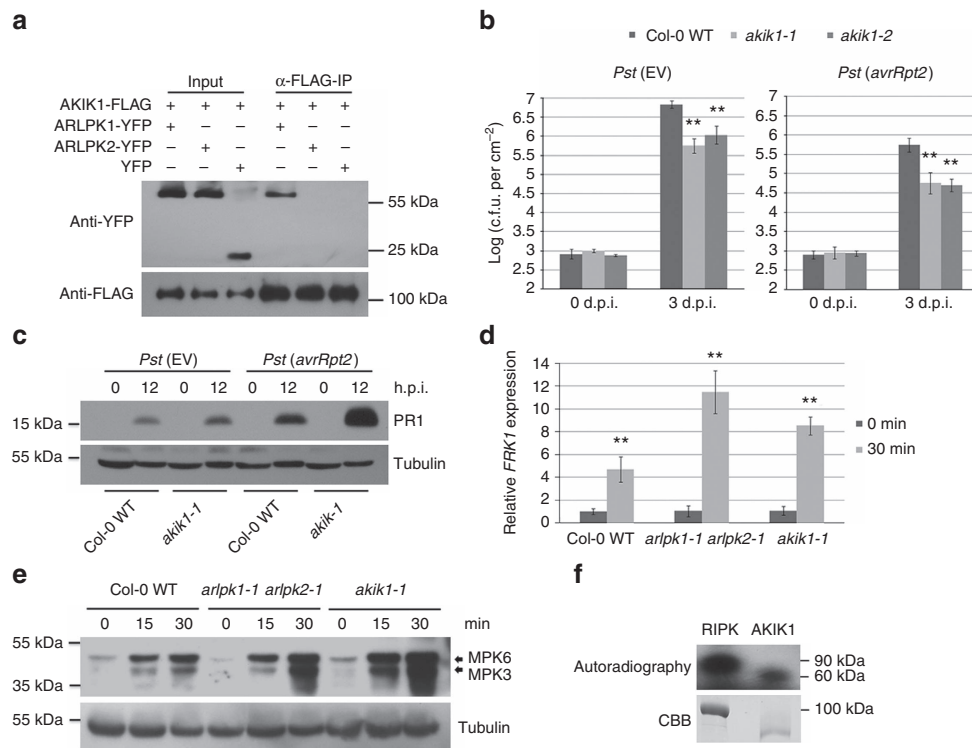


Figure 6 | ARLPK1 interacts with AKIK1 that is also a negative regulator of disease resistance. (a) AKIK1-FLAG co-IP with ARLPK1-YFP but not with ARLPK2-YFP. Total proteins (input) from *N. benthamiana* extracts were immunoprecipitated with ANTI-FLAG M2 affinity gel, and AKIK1-FLAG and ARLPK1-YFP proteins were detected by western blot using anti-FLAG and anti-YFP antibodies, respectively. Similar results were obtained from three biological replicates. (b) The *akik1-1* and *akik1-2* mutants are more resistance to bacterial *Pst* (EV) and *Pst* (*avrRpt2*), as compared with WT plants. Bacterial inoculum concentration: 5×10^5 c.f.u. per ml. Bacterial growth was measured 3 d.p.i. Error bars represent s.d. for at least 15 leaf discs. Similar results were obtained from three biological replicates. ***P* value < 0.01 (Student's *t*-test). (c) PR1 protein levels in *Pst* (EV)- and *Pst* (*avrRpt2*)-infected Col-0 WT and *akik1-1* mutant were detected by western blot using an anti-PR1 antibody. Bacterial inoculum concentration: 1×10^7 c.f.u. per ml. Leaf tissue was collected 0 and 12 h.p.i. α -Tubulin was used as a loading control. Similar results were obtained from two biological replicates. (d) Relative expression levels of *FRK1* in flg22-treated Col-0 WT, *arlpk1-1 arlpk2-1* and *akik1-1* mutants were detected by real-time RT-PCR. Samples were collected 0 and 30 min after treatment. Error bars indicate s.d. from three technical replicates. Similar results were obtained from three biological replicates. ***P* value < 0.01 (Student's *t*-test). (e) The levels of phosphorylated MPK3 and MPK6 in flg22-treated Col-0 WT, *arlpk1-1 arlpk2-1* and *akik1-1* mutants were detected by western blot using monoclonal rabbit phospho-p44/42 MAPK (Erk1/2) (Thr202/Tyr204)(D13.14.4E) XP antibody. Leaf tissue was collected 0, 15 and 30 min after treatment. α -Tubulin was used as a loading control. Similar results were obtained from three biological replicates. (f) Recombinant MBP-tagged RIPK kinase domain and GST-tagged AKIK1 kinase domain were subjected to a radioactive kinase assay and kinase activity was detected using autoradiography. Bottom panel: SDS-PAGE gel stained with coomassie brilliant blue (CBB) demonstrating protein abundance. Similar results were obtained from two biological replicates.

SE is a positive regulator of plant immunity. SE was originally identified as a C₂H₂-type zinc-finger protein important in leaf and meristem development, inflorescence architecture and phase transition^{28,35}. Since then, it has been shown to play a role in a crucial step of miRNA maturation and accumulation^{18–21}, pre-mRNA splicing³⁶ and alternative splicing²⁴. We hypothesized that as a target of miR863, SE should have a role in disease resistance; however, nothing has been uncovered so far regarding its function in antibacterial defence in plants.

We obtained the *se-1* mutant (CS3257), which contains an X-ray-induced 7-base deletion, for analysis^{21,28,35}. The *se-1* mutant is smaller, has serrated leaves and exhibits pleiotropic defects in shoot and leaf development²⁸. We inoculated the *se-1* plants with *Pst* (EV), *Pst* (*avrRpt2*) and a mock solution to determine the role of SE in disease resistance. The *se-1* mutant showed increased disease susceptibility manifested as stronger chlorosis, or yellowing of the leaves, 3–4 d.p.i. (days post inoculation) compared with Col-0 WT plants. Infection with pathogen does not stunt growth of *se-1* mutants (Fig. 7a). The *se-1* mutant also showed delayed HR after infection with *Pst*

(*avrRpt2*), indicating a weaker or slower RPS2-mediated defence response against *Pst* (*avrRpt2*) (Fig. 7b). We included *Pst* (EV) infection as a control, which did not trigger HR; however, at 48 h.p.i., the *se-1* mutant showed chlorosis of the leaves (Fig. 7b) while Col-0 WT did not. We also measured the bacterial titre in *se-1* mutant and found that both *Pst* (EV) and *Pst* (*avrRpt2*) growth was greater in the mutants compared with Col-0 WT plants (Fig. 7c). Consistent with the bacterial growth assays, PR1 protein expression is lower in *se-1* mutant than in Col-0 WT after infection with *Pst* (EV) and *Pst* (*avrRpt2*) (Fig. 7d). *FRK1* transcript level (Fig. 7e) and MPK6 and MPK3 protein levels (Fig. 7f) are lower in *se-1* after flg22 treatment than in Col-0 WT. Furthermore, we obtained *Arabidopsis* transgenic lines overexpressing SE CDS in the *se-1* background^{21,24} (SE-OE) that have a complemented leaf phenotype and are slightly smaller than Col-0 WT plants (Fig. 7g). We confirmed the overexpression of SE in these lines (Fig. 7h), and found that they show enhanced disease resistance to *Pst* (EV) and *Pst* (*avrRpt2*) (Fig. 7i). Taken together, these data further support SE is a positive regulator of disease resistance.

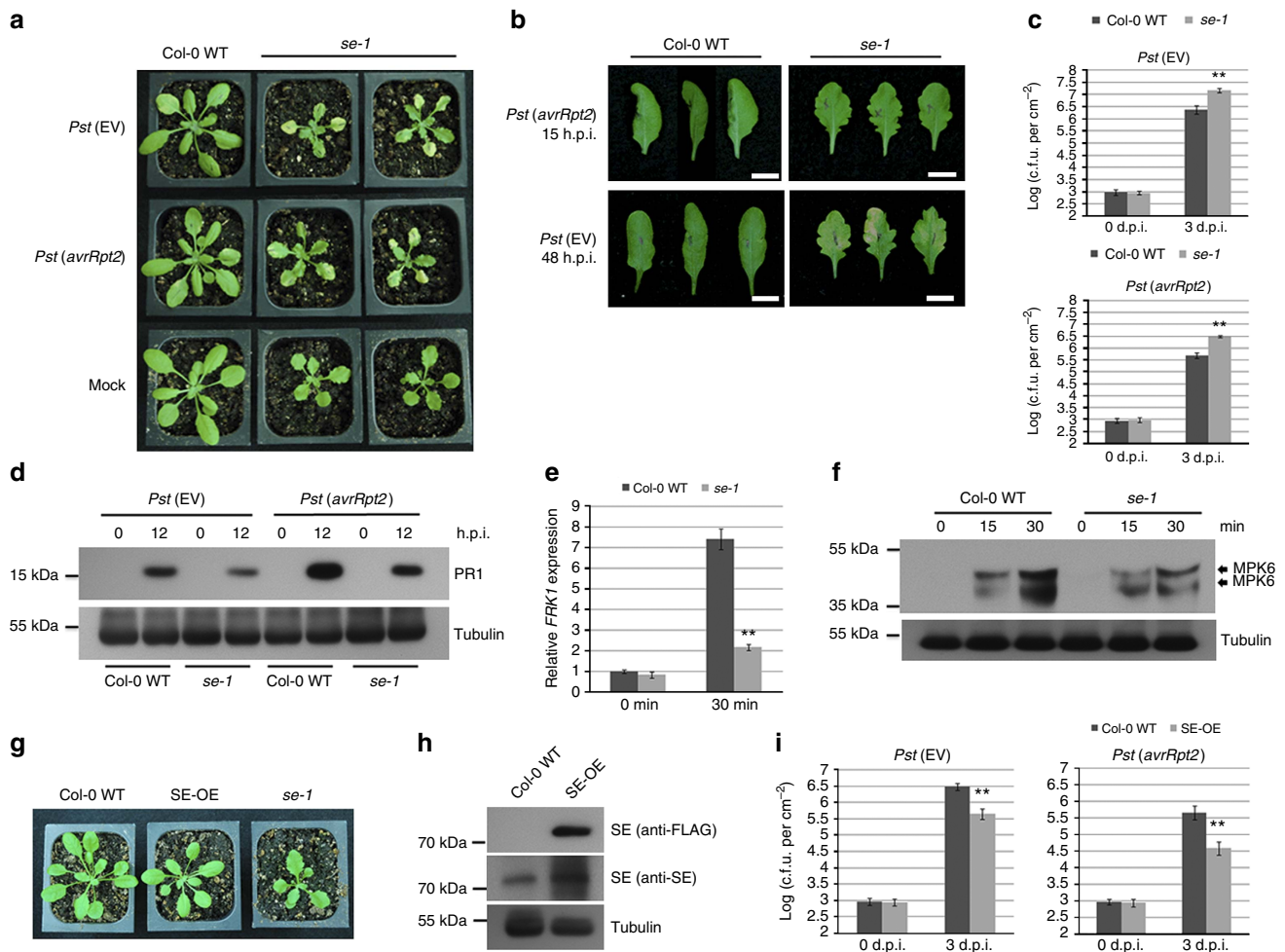


Figure 7 | SE is a positive regulator of disease resistance. (a) The *se-1* mutant displays enhanced disease susceptibility phenotype after *Pst* (EV) and *Pst* (*avrRpt2*) infection. Bacterial inoculum concentration: 5×10^5 c.f.u. per ml. Photos were taken 3 d.p.i. Mock-treated plants were used as controls. (b) The *se-1* mutant shows delayed HR after *Pst* (*avrRpt2*) infection, and enhanced disease phenotype after *Pst* (EV) infection. Pictures were taken 15 h.p.i. of *Pst* (*avrRpt2*) infection and 48 h.p.i. of *Pst* (EV) infection. In all, 16 out of 18 *Pst* (*avrRpt2*)-infected Col-0 WT leaves exhibited HR at 15 h.p.i. under our conditions (three with HR are shown), while only 3 out of 18 of the *se-1* leaves showed HR at 16 h.p.i. (three without HR are shown). A total of 12 out of 15 *Pst* (*avrRpt2*)-infected *se-1* leaves exhibited chlorosis, while only 3 out of 15 Col-0 WT leaves did. Only half of the leaf was inoculated. Bacterial inoculum concentration: 1×10^7 c.f.u. per ml. Scale bar, 10 mm. (c) The *se-1* mutant is more susceptible to the infection of *Pst* (EV) and *Pst* (*avrRpt2*) than Col-0 WT. Bacterial inoculum concentration: 5×10^5 c.f.u. per ml. Bacterial growth was measured 3 d.p.i. Error bars represent s.d. for at least 15 leaf discs. Similar results were obtained from three biological replicates. ***P* value < 0.01 (Student's *t*-test). (d) PR1 protein levels in *Pst* (EV)- and *Pst* (*avrRpt2*)-infected Col-0 WT and *se-1* mutants were detected by western blot using an anti-PR1 antibody. Bacterial inoculum concentration: 1×10^7 c.f.u. per ml. Leaf tissue was collected 0 and 12 h.p.i. α -Tubulin was used as a loading control. Similar results were obtained from two biological replicates. (e) Relative expression levels of *FRK1* in flg22-treated Col-0 WT and *se-1* mutant were detected by real-time RT-PCR. Leaf tissue was collected 0 and 30 min after treatment. Error bars indicate s.d. from three technical replicates. Similar results were obtained in three biological replicates. ***P* value < 0.01 (Student's *t*-test). (f) MPK3 and MPK6 protein levels in flg22-treated Col-0 WT and *se-1* mutant were detected by western blot using monoclonal rabbit phospho-p44/42 MAPK (Erk1/2) (Thr202/Tyr204)(D13.14.4E) XP antibody. Samples were collected 0, 15 and 30 min after treatment. α -Tubulin was used as a loading control. Similar results were obtained from two biological replicates. (g) Phenotypes of 4-week-old FLAG-tagged SE overexpression lines (SE-OE), *se-1* mutants and Col-0 WT plants. (h) SE protein levels were detected in Col-0 WT and FLAG-tagged SE-OE lines by western blot using anti-FLAG and anti-SE antibodies. α -Tubulin was used as a loading control. Similar results were obtained from two biological replicates. (i) Bacterial growth in *Pst* (EV)- and *Pst* (*avrRpt2*)-infected Col-0 WT and SE-OE lines. Bacterial inoculum concentration: 5×10^5 c.f.u. per ml. Bacterial growth was measured 3 d.p.i. Error bars represent s.d. for at least 15 leaf discs. Similar results were obtained from three biological replicates. ***P* value < 0.01 (Student's *t*-test).

miR863 sequentially silences its targets to regulate defence.

Our results showed that the three confirmed targets of miR863 have opposite roles in plant immunity. While the ARLPKs are negative regulators of defence, SE is a positive regulator, thus explaining why overexpressing miR863 has no clear effect on disease resistance (Fig. 3e). Thus far, known miRNAs involved in immunity target either negative or positive regulators of plant immunity, not both. To find out why miR863-3p silences targets with opposite cellular functions, we performed a time course

experiment and examined the levels of the targets during early and late stages after infection with *Pst* (*avrRpt2*). Because high inoculum concentration of avirulent *Pst* can trigger HR and thus affect the expression levels of many genes, we used a lower concentration (2×10^6 colony-forming units (c.f.u.) per ml) that would not trigger macroscopic HR at 15 h.p.i., but could still induce miR863-3p levels. Real-time RT-PCR and western blot analysis revealed the kinases are downregulated early, just at 4 h.p.i. (Fig. 8a), while SE protein levels are downregulated much

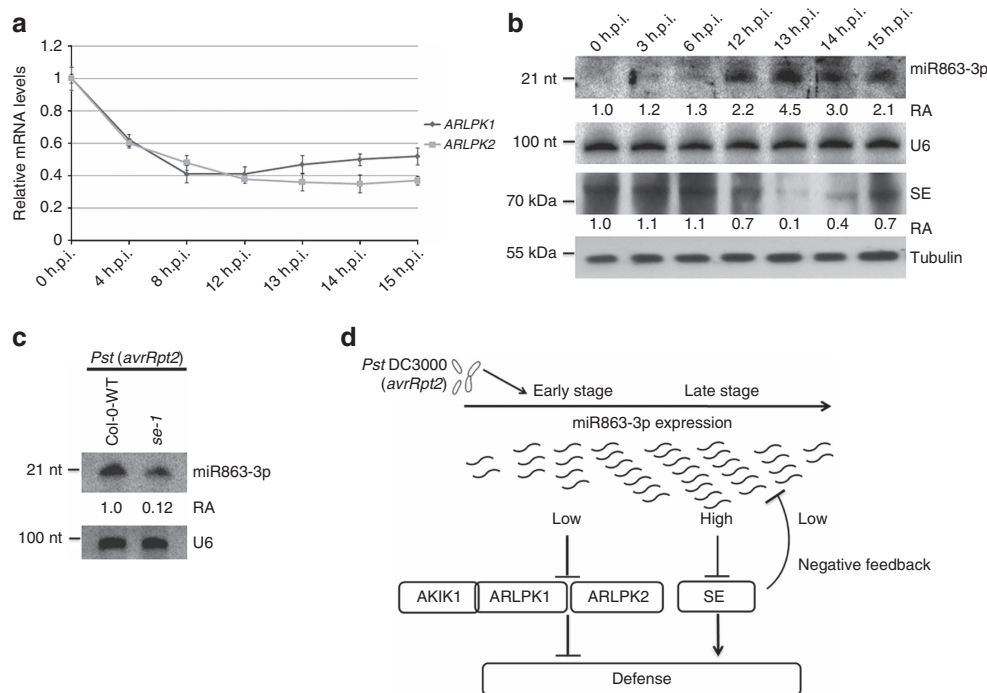


Figure 8 | miR863-3p regulates ARLPK1, ARLPK2 and SE in a time-dependent manner. (a) Time course of relative expression levels of *ARLPK1* and *ARLPK2* transcripts in *Pst (avrRpt2)*-infected Col-0 WT plants were detected by real-time RT-PCR. Bacterial inoculum concentration: 5×10^6 c.f.u. per ml. Error bars indicate s.d. from three technical replicates. Similar results were obtained in three biological replicates. $**P$ value < 0.01 (Student's *t*-test). (b) Time course of miR863-3p levels in *Pst (avrRpt2)*-infected Col-0 WT plants was detected by northern blot analysis. U6 was used as a loading control. SE protein levels in *Pst (avrRpt2)*-inoculated Col-0 WT plants were detected by western blot analysis using an anti-SE antibody. α -Tubulin was used as a loading control. Relative abundance (RA) levels are indicated. Bacterial inoculum concentration: 5×10^6 c.f.u. per ml. Similar results were obtained from two biological replicates. (c) miR863-3p levels in *Pst (avrRpt2)*-infected Col-0 WT and *se-1* mutants were detected by northern blot analysis. U6 was used as a loading control. Bacterial inoculum concentration: 1×10^7 c.f.u. per ml. Samples were collected 14 h.p.i. RA levels are indicated. Similar results were obtained from three biological replicates. (d) A model of miR863-3p downregulation of targets after infection with *Pst (avrRpt2)*. During the early stage of infection, miR863-3p levels are upregulated and suppress *ARLPK1* and *ARLPK2* to enhance disease resistance. *ARLPK1* interacts with LRR-RLK *AKIK1* to negatively regulate defence. During the later stage of infection, miR863-3p downregulates *SE*. Downregulation of *SE* results in a decrease in miR863-3p levels, forming a negative feedback loop to suppress defence responses.

later, around 12 h.p.i. (Fig. 8b). It may be that *SE* is not targeted by miR863 during earlier stages of infection because a higher level of miR863 is required for translation inhibition of *SE*, which is not achieved until the late stage of infection. After *SE* protein levels decrease, the accumulation of miR863-3p also decreases in the later stages of infection (Fig. 8c). We probed miR393 and miR319 as well and found that the levels of both also decrease in latter stages of infection similar to that of miR863-3p, showing that downregulation of *SE* protein does indeed affect miRNA accumulation (Supplementary Fig. 9a). We also performed the time course experiment with *Pst* (EV) infection and found that the levels of *ARLPK1* and *ARLPK2* mRNA, miR863-3p and *SE* protein did not significantly change over time (Supplementary Fig. 9b). These results show that miR863-3p temporal regulation of its targets is more predominant in ETI, although *ARLPK1*, *ARLPK2* and *AKIK1* all have roles in negative regulation of both ETI and PTI.

Discussion

The initiation, timing and amplitude of plant defence responses are tightly controlled. Cellular reprogramming that occurs during pathogen infection is energy consuming; thus, a trade-off exists between plant growth and defence³⁷. In recent years, several miRNAs and siRNAs with important roles in plant immunity have been discovered. However, no sRNAs that target genes with antagonistic roles in response to the same environmental or developmental cues have been reported in any

cellular processes within any organisms. Here we identified miR863-3p, which is highly induced by *Pst (avrRpt2)* infection and sequentially silences negative and positive regulators of plant immunity through two different modes of action. miR863-3p first suppresses negative regulators—*ARLPK1* and *ARLPK2*—via mRNA degradation to boost defence responses quickly after infection. *ARLPK1* interacts with *AKIK1*, which also functions as a negative regulator. Then, during later stages of infection, miR863-3p downregulates *SE* via translational inhibition to attenuate defence signalling by bringing down the level of miR863-3p, of which accumulation is dependent on *SE* (Fig. 8c,d), thus forming a negative feedback loop to attenuate plant immunity. Thus, miR863-3p plays a critical role in regulating and fine-tuning the timely upregulation of plant defences on pathogen infection, as well as the attenuation of immune responses after successful defence. Just as the timely upregulation of plant defences on pathogen infection is crucial for survival, the attenuation of immune responses after successful defence may also be important to conserve host resources for growth and reproduction.

Even though miR863-3p regulates *ARLPK1*, *ARLPK2* and *SE* during ETI, all targets, as well as *AKIK1*, are regulators of not only ETI but also PTI. A recent systematic study of network characteristics in ETI and PTI revealed that both share a large subnetwork of genes and interactors that most likely functions to favour plant defence over growth³⁸. However, the organization of defence response modules in ETI is independent, rather than

cohesive as it is in PTI, due to the evolutionary demand for a rapid and robust response to pathogen effectors³⁸.

The RLK/Pelle family has over 600 members and is the largest group of protein kinases in *Arabidopsis*²³. Many RLKs are extensively involved in signalling pathways in development and plant immunity^{39–41}. In the recent years, several RLKs that play a role in negative regulation of plant defence have been discovered, such as growth-promoting phytosulfokine (PSK) receptors PSKR1 and PSY1R (refs 42,43), and BAK1-interactors BIR1 (ref. 44) and BIR2 (ref. 45). Interestingly, the BIR2 kinase domain is missing conserved motifs and exhibits no kinase activity⁴⁵. Nearly 20% of *Arabidopsis* RLKs are predicted to be pseudokinases and can have phosphorylation-independent mechanisms of mediating signal transduction⁴⁶. Many pseudo-kinases have important functions in humans⁴⁷, plants^{48–51} and bacteria^{52,53}, and still possess kinase catalytic activity or bind nucleotides and/or cations. They can act as scaffolding proteins or regulate the activity of functional kinases²⁵. Neither ARLPK1 nor ARLPK2 exhibited detectable autophosphorylation *in vitro* (Fig. 4f) and may thus function as scaffolding proteins or modulate the activity of AKIK1 or other kinases to regulate immune signalling.

Most studied RLKs, including PSKY1 (ref. 54), PSY1R (ref. 55), BIR1 (ref. 44) and BIR2 (ref. 45), localize in the plasma membrane, but we found that ARLPK1, ARLPK2 and AKIK1 were all predominantly localized to the ER (Fig. 5 and Supplementary Fig. 6). ARLPK1 and ARLPK2 both have predicted signal peptides that overlap with their transmembrane domains (Supplementary Fig. 2); thus, it is possible that the sequences are not true signal peptides. In contrast, AKIK1 has a clear signal peptide (Supplementary Fig. 7). It is possible that AKIK1 also localizes in other cellular organelles. Future experiments would involve obtaining native antibodies specific to AKIK1, ARLPK or ARLPK2, to determine their subcellular localization *in vivo*. The multigene family of hormone ethylene receptor kinases—including ETR1, ERS1, CTR1 and EIN2—are ER-membrane bound. Ethylene plays a role in many plant growth and development processes, as well as responses to environmental stresses, and its gaseous nature may explain why its receptors can localize in the ER⁵⁶. *Arabidopsis* hormone cytokinin receptors—AHK2, AHK3 and CRE1/AHK4—which play roles in plant growth and formation, as well as in biotic and abiotic stress responses, are all membrane-bound kinases that mainly localize in the ER. These receptors may be localized in the ER for crosstalk or for close proximity to the nucleus for downstream signalling⁵⁷. On the other hand, *Arabidopsis* AtIre1-1 and AtIre1-2 are transmembrane receptor kinases located in the ER and most likely function in ER unfolded protein response signalling, like their yeast and mammalian homologue Ire1 (ref. 58). How the roles of ARLPK1, ARLPK2 and AKIK1 are related to their subcellular localization in the ER remains to be determined. Finding their downstream components or other interacting partners may shed light on this question.

The role of SE in antibacterial plant defence has not been previously uncovered. However, *dcl1*, *hyl1* and *hen1*, the mutants defective in miRNA accumulation, have decreased basal defence^{12,14}. One study showed that SE might be involved in the cuticle integrity pathway, and related to that, *se-1* mutants are more susceptible to necrotrophic fungal infection⁵⁹. SE has been proposed to regulate gene expression by modifying chromatin structure³⁵. As a component of the nuclear cap-binding complex, SE also has a role in pre-mRNA splicing³⁶. This distinguishes SE from DCL1 and HYL1, which participate in only miRNA processing²⁴. Other SE-dependent miRNAs are also likely to be involved during later infection stages to returning the host immune system to a normal state. Future research focusing on the

role of additional SE-related miRNAs as well as ARLPK1 and ARLPK2 targets will enhance our understanding of temporal immune signalling.

Methods

Plant materials and growth conditions. *Arabidopsis* and *N. benthamiana* plants were grown in a controlled growth room at 23 ± 1 °C in a 12-h light/12-h dark photoperiod. All experiments were performed on 4-week-old *Arabidopsis* plants and 3-week-old *N. benthamiana* plants. The following mutants seeds were used in this study: *dcl1-7/fwf2* (ref. 13), *rdr6-15* (ref. 60), *se-1* (ref. 28), and SALK lines *arlpk-1* (SALK_144635), *arlpk-1* (SALK_040744), *akik1-1* (SALK_022711C) and *akik1-2* (CS848612)²⁹. Homozygous mutant plants were identified by RT-PCR, and primers are listed in Supplementary Table 1. All mutants were in the Columbia (Col-0) background, except for *dcl1-7/fwf2*, which was in the Landsberg *erecta* (Ler) background.

Identification of target proteins of miR863. To identify miR863-3p target genes, a set of computational rules for target prediction was adapted from Allen *et al.*⁶¹ and modified. The miRNA-target duplex must contain four or less unpaired bases, four or less G:U pairs, up to one single-nucleotide bulge and seven or fewer unpaired plus G:U positions. Nucleotides at positions 10 and 11 of the miRNA must be a perfect match with its target. Mismatched pairs or single-nucleotide bulges were given a score of 1; G:U pairs were given a score of 0.5. Mismatched and G:U pair scores were doubled if they were located within the core segment (positions 2–13). A maximum of three continuous mismatches was allowed if the mismatch region contained at least two G:U pairs, and the penalty score of the region was multiplied by 1.5. We used 5.5 as the cutoff score for selecting the miRNA targets.

Bacterial infection. Bacterial strains used include the following: *Pseudomonas syringae* pv. *tomato* DC3000 carrying broad host range vector pVSP61 (ref. 62) (EV); or pVSP61 plasmid containing avirulence gene *avrRpt2* (ref. 62), *avrRpm1* (ref. 63) or *avrRps4* (ref. 64); and a strain that has a mutation in its type III secretion system (*ΔhrcC*)⁶⁵. For bacterial growth assays, 4-week-old *Arabidopsis* plants were syringe-infiltrated with a 5 × 10⁵ c.f.u. per ml bacterial suspension. Leaves were collected 3 d.p.i. using a cork borer, and bacterial titre was determined by serial dilution, plating and counting the colonies. At least 15 leaf discs were collected for each growth assay. Three biological repeats were performed with similar results. Student's *t*-test was used to determine the significant differences between mutants and control plants. For northern and western blots and the HR assay, a 1 × 10⁷ c.f.u. per ml bacterial suspension was used. A total of 18 leaves were infected for the HR assay and monitored for the appearance of HR symptoms. For the time course, a 2 × 10⁶ c.f.u. per ml bacterial suspension was used.

Generation of transgenic plants. To generate the construct for the MIR863-OE lines, the miR863 precursor was cloned using a miR319 backbone⁶⁶ into a pEarleyGate (pEG) 100 destination vector⁶⁷ using LR clonase II (Invitrogen). To generate the mARLPK1-OE lines, the mutated (m) ARLPK1 CDS was cloned into pEG104. *Arabidopsis* plants were transformed using floral dip method with *Agrobacterium tumefaciens* strain GV3101 carrying the carrying cloned vectors.

Protein extraction and analysis. Tissue sample was ground in liquid nitrogen and total proteins were extracted using 2 × SDS loading buffer. The samples were resolved on a 12% SDS-PAGE gel and transferred onto nitrocellulose membranes using a Tris-Glycine transfer buffer. The blots were probed with the appropriate antibodies: monoclonal mouse anti-GFP, which also recognizes YFP (Roche, 11814460001, 1:2,000 dilution); monoclonal mouse anti-FLAG (Sigma-Aldrich, F3165, 1:2,000 dilution); monoclonal mouse anti- α tubulin (Sigma-Aldrich, T6074, 1:4,000 dilution); polyclonal rabbit anti-PR1 (obtained from Xinnian Dong⁶⁸, 1:2,000 dilution); polyclonal rabbit anti-SE (serum containing polyclonal antibodies was produced in rabbits immunized with peptide containing the first 200 amino acids of the SE protein, AbMax Biotechnology Co., Ltd., 1:1,000 dilution); rabbit serum was purified using Montage Antibody Purification kit, Millipore); goat anti-mouse IgG-HRP (Santa Cruz Biotechnology, sc-2005, 1:4,000 dilution); and goat anti-rabbit IgG-HRP (Santa Cruz Biotechnology, sc-2030, 1:4,000 dilution).

Transient expression analysis in *N. benthamiana*. Transient co-expression and co-immunoprecipitation assays in *N. benthamiana* were performed by infiltrating 3-week-old *N. benthamiana* plants with *Agrobacterium* (OD₆₀₀ (optical density at 600 nm) = 1.0) harbouring constructs containing the miR863 precursor with *Agrobacterium* containing (OD₆₀₀ = 1.0) wtARLPK1 or mutated (m) ARLPK1 CDS (pEG104), wtARLPK2 or mARLPK2 CDS (pEG104), and GFP-wtSE-3'-UTR or GFP-mSE-3'-UTR (pEG103). Leaf tissue was collected 48 h.p.i. and processed as described above. AKIK1 (pEG202) was used for Co-IP assays with ARLPK1 and ARLPK2. ANTI-FLAG M2 affinity gel (Sigma-Aldrich, A2220) was used for pull downs.

5'-RACE of mRNA cleavage products. 5'-RACE⁶⁹ was performed using FirstChoice RLM-5'-RACE kit (Ambion) following the manufacturer's instructions. Briefly, total RNA was extracted from *Pst* (*avrRpt2*)-infected tissue 10 h.p.i. and directly ligated to the RNA Oligo adaptor without further modification. Oligo (dT) primer was used to prime cDNA synthesis with reverse transcriptase. Gene-specific 5'-RACE reactions were done with the 5' Nested Primer and gene-specific primers ARLPK1-R 5'-RACE and ARLPK2-R 5'-RACE as listed in Supplementary Table 1. The 5'-RACE products were gel purified, cloned into pENTR (Invitrogen) vector and sequenced.

Site-directed mutagenesis. The wtARLPK1 CDS, ARLPK2 CDS and SE 3'-UTR sequences were cloned into pENTR (Invitrogen) vector. Point mutations were introduced using the GeneArt Site-Directed Mutagenesis System kit (Invitrogen) following the manufacturer's instructions. Primers used are listed in Supplementary Table 1 as mARLPK1-F, mARLPK1-R, mARLPK2-F, mARLPK2-R, mSE 3'-UTR-F and mSE 3'-UTR-R. The final plasmids with the mutated sequences were cloned into the pEG104 (mARLPK1 and mARLPK2) or pEG103 (mSE-3'-UTR) destination vectors using LR Clonase II (Invitrogen).

Protein kinase assays. ARLPK1 and ARLPK2 were cloned into pMAL-C4X with N-terminal fusions to maltose-binding protein (MBP). MBP-ARLPK1, MBP-ARLPK2 and MBP-RIPK were induced with 0.3 mM isopropyl-β-D-thiogalactoside for 3 h at 28 °C and purified by amylose affinity chromatography from *E. coli*. The kinase domain of AKIK1 (547–892 aa) was cloned into pDEST-15 (Invitrogen) with an N-terminal fusion to glutathione S-transferase (GST). GST-AKIK1 was expressed in *E. coli* (BL21 strain) at 28 °C for 4 h and the recombinant protein purified with Glutathione Sepharose 4B (GE Healthcare). Kinase assays were performed using 3 μg of recombinant protein with [³²P]-ATP. The assay was initiated by adding 1 ml (10 μCi) ³²P-ATP and incubated for 40 min at 30 °C. The reaction was terminated by the addition of 3 × laemmli loading buffer and subsequent incubation at 95 °C for 5 min. The proteins were separated on a 12% SDS-PAGE gel and signals were visualized by X-ray film exposure³⁰.

RNA extraction and analysis. Fresh tissue was ground in liquid nitrogen and RNA was extracted using TRIzol Reagent (Invitrogen) following the manufacturer's instructions. RNA is resolved on a 17% denaturing 8 M urea-PAGE gel and then transferred and chemically crosslinked onto a Hybond N⁺ membrane (GE Healthcare Life Sciences) using *N*-(3-Dimethylaminopropyl)-*N'*-(3-Dimethylaminopr hydrochloride, miRNAs were detected using end-labelled oligonucleotide probes and exposed to a phosphor imager screen. ImageQuant TL 7.0 analysis software (GE Healthcare Life Sciences) was used to measure relative abundance levels. For quantification of relative gene expression, cDNA was synthesized using Superscript III (Invitrogen), and real-time RT-PCR was performed using SYBR green dye (Bio-Rad) on a MyiQ detection system (Bio-Rad). The primers for all experiments are listed in Supplementary Table 1.

MAPK activity assay. Two-week-old seedlings grown on half-strength Murashige and Skoog medium were treated with 10 μM flg22 containing 0.01% Silwet L-77. Samples were collected at 0, 5, 10, 15 and 30 min, and analysed by western blotting using monoclonal rabbit phospho-p44/42 MAPK (Erk1/2) (Thr202/Tyr204) (D13.14.4E) XP antibodies (Cell Signaling Technology, #4370S, 1:2,000 dilution). α-tubulin was used as a loading control using monoclonal mouse anti-α tubulin (Sigma-Aldrich, T6074, 1:4,000 dilution).

Subcellular localization. Subcellular localization of fluorescent-tagged proteins was determined using confocal microscopy. Three-week-old *N. benthamiana* plants were infiltrated with *Agrobacterium* carrying constructs ARLPK1-YFP, ARLPK2-YFP, AKIK1-CFP, RLK-CFP, ER-mCherry (ER-rk; CD3-959) or empty GFP vector. Untreated tissue was collected 48 h.p.i. Plants were treated with *Pst* (*avrRpt2*) 48 h.p.i. after infiltration with *Agrobacterium* and tissue was collected 12 h.p.i. For the plasmolysis treatment, tissue was treated with 5% NaCl for 5–10 min before visualization (+NaCl), or with water as a control (–NaCl). The ER marker is the mCherry fluorescent protein with the signal peptide of *Arabidopsis* wall-associated kinase 2 (AtWAK2) at the N terminus and the ER retention signal His-Asp-Glu at the C terminus³¹. The plasma membrane marker is an RLK (At4g23740) fused to CFP at the C terminus⁷⁰.

Full uncropped versions of each gel and blot image are included in Supplementary Fig. 10. Results for biological replicates are included in Supplementary Fig. 11.

References

- Katiyar-Agarwal, S. & Jin, H. Role of small RNAs in host-microbe interactions. *Annu. Rev. Phytopathol.* **48**, 225–246 (2010).
- Weiberg, A. & Jin, H. Small RNAs—the secret agents in the plant-pathogen interactions. *Curr. Opin. Plant Biol.* **26**, 87–94 (2015).
- Weiberg, A., Wang, M., Bellinger, M. & Jin, H. Small RNAs: a new paradigm in plant-microbe interactions. *Annu. Rev. Phytopathol.* **52**, 495–516 (2014).
- Padmanabhan, C., Zhang, X. & Jin, H. Host small RNAs are big contributors to plant innate immunity. *Curr. Opin. Plant Biol.* **12**, 465–472 (2009).
- Macho, A. P. & Zipfel, C. Plant PRRs and the activation of innate immune signaling. *Mol. Cell* **54**, 263–272 (2014).
- Dodds, P. N. & Rathjen, J. P. Plant immunity: towards an integrated view of plant-pathogen interactions. *Nat. Rev. Genet.* **11**, 539–548 (2010).
- Li, X., Kapos, P. & Zhang, Y. NLRs in plants. *Curr. Opin. Immunol.* **32**, 114–121 (2015).
- Kunkel, B. N., Bent, A. F., Dahlbeck, D., Innes, R. W. & Staskawicz, B. J. RPS2, an Arabidopsis disease resistance locus specifying recognition of *Pseudomonas syringae* strains expressing the avirulence gene *avrRpt2*. *Plant Cell* **5**, 865–875 (1993).
- Yu, G. L., Katagiri, F. & Ausubel, F. M. Arabidopsis mutations at the Rps2 locus result in loss of resistance to *Pseudomonas-Syringae* strains expressing the avirulence gene *AvrRpt2*. *Mol. Plant Microbe In.* **6**, 434–443 (1993).
- Weiberg, A. *et al.* Fungal small RNAs suppress plant immunity by hijacking host RNA interference pathways. *Science* **342**, 118–123 (2013).
- Martinez de Alba, A. E., Elvira-Matlot, E. & Vaucheret, H. Gene silencing in plants: a diversity of pathways. *Biochim. Biophys. Acta* **1829**, 1300–1308 (2013).
- Katiyar-Agarwal, S. *et al.* A pathogen-inducible endogenous siRNA in plant immunity. *Proc. Natl Acad. Sci. USA* **103**, 18002–18007 (2006).
- Katiyar-Agarwal, S., Gao, S., Vivian-Smith, A. & Jin, H. A novel class of bacteria-induced small RNAs in Arabidopsis. *Genes Dev.* **21**, 3123–3134 (2007).
- Navarro, L. *et al.* A plant miRNA contributes to antibacterial resistance by repressing auxin signaling. *Science* **312**, 436–439 (2006).
- Zhang, X. *et al.* Arabidopsis Argonaute 2 regulates innate immunity via miRNA393 (*)-mediated silencing of a Golgi-localized SNARE gene, MEMB12. *Mol. Cell* **42**, 356–366 (2011).
- Li, Y. *et al.* Identification of microRNAs involved in pathogen-associated molecular pattern-triggered plant innate immunity. *Plant Physiol.* **152**, 2222–2231 (2010).
- Zhang, W. *et al.* Bacteria-responsive microRNAs regulate plant innate immunity by modulating plant hormone networks. *Plant Mol. Biol.* **75**, 93–105 (2011).
- Yang, L., Liu, Z. Q., Lu, F., Dong, A. W. & Huang, H. SERRATE is a novel nuclear regulator in primary microRNA processing in Arabidopsis. *Plant J.* **47**, 841–850 (2006).
- Fang, Y. & Spector, D. L. Identification of nuclear dicing bodies containing proteins for microRNA biogenesis in living Arabidopsis plants. *Curr. Biol.* **17**, 818–823 (2007).
- Dong, Z., Han, M. H. & Fedoroff, N. The RNA-binding proteins HYL1 and SE promote accurate in vitro processing of pri-miRNA by DCL1. *Proc. Natl Acad. Sci. USA* **105**, 9970–9975 (2008).
- Lobbess, D., Rallapalli, G., Schmidt, D. D., Martin, C. & Clarke, J. SERRATE: a new player on the plant microRNA scene. *EMBO Rep.* **7**, 1052–1058 (2006).
- Meyers, B. C. *et al.* Criteria for annotation of plant MicroRNAs. *Plant Cell* **20**, 3186–3190 (2008).
- Shiu, S. H. *et al.* Comparative analysis of the receptor-like kinase family in Arabidopsis and rice. *Plant Cell* **16**, 1220–1234 (2004).
- Raczynska, K. D. *et al.* The SERRATE protein is involved in alternative splicing in Arabidopsis thaliana. *Nucleic Acids Res.* **42**, 1224–1244 (2014).
- Boudeau, J., Miranda-Saavedra, D., Barton, G. J. & Alessi, D. R. Emerging roles of pseudokinases. *Trends Cell Biol.* **16**, 443–452 (2006).
- Rogers, K. & Chen, X. Biogenesis, turnover, and mode of action of plant microRNAs. *Plant Cell* **25**, 2383–2399 (2013).
- Liu, J. D., Valencia-Sanchez, M. A., Hannon, G. J. & Parker, R. MicroRNA-dependent localization of targeted mRNAs to mammalian P-bodies. *Nat. Cell Biol.* **7**, 719–U118 (2005).
- Clarke, J. H., Tack, D., Findlay, K., Van Montagu, M. & Van Lijsebettens, M. The SERRATE locus controls the formation of the early juvenile leaves and phase length in Arabidopsis. *Plant J.* **20**, 493–501 (1999).
- Alonso, J. M. *et al.* Genome-wide insertional mutagenesis of Arabidopsis thaliana. *Science* **301**, 653–657 (2003).
- Liu, J., Elmore, J. M., Lin, Z. J. & Coaker, G. A receptor-like cytoplasmic kinase phosphorylates the host target RIN4, leading to the activation of a plant innate immune receptor. *Cell Host Microbe* **9**, 137–146 (2011).
- Nelson, B. K., Cai, X. & Nebenfuhr, A. A multicolored set of in vivo organelle markers for co-localization studies in Arabidopsis and other plants. *Plant J.* **51**, 1126–1136 (2007).
- Robatzek, S., Chinchilla, D. & Boller, T. Ligand-induced endocytosis of the pattern recognition receptor FLS2 in Arabidopsis. *Genes Dev.* **20**, 537–542 (2006).
- Geisler-Lee, J. *et al.* A predicted interactome for Arabidopsis. *Plant Physiol.* **145**, 317–329 (2007).
- Asai, T. *et al.* MAP kinase signalling cascade in Arabidopsis innate immunity. *Nature* **415**, 977–983 (2002).

35. Prigge, M. J. & Wagner, D. R. The arabidopsis serrate gene encodes a zinc-finger protein required for normal shoot development. *Plant Cell* **13**, 1263–1279 (2001).
36. Laubinger, S. *et al.* Dual roles of the nuclear cap-binding complex and SERRATE in pre-mRNA splicing and microRNA processing in Arabidopsis thaliana. *Proc. Natl Acad. Sci. USA* **105**, 8795–8800 (2008).
37. Belkadir, Y., Yang, L., Hetzel, J., Dangl, J. L. & Chory, J. The growth-defense pivot: crisis management in plants mediated by LRR-RK surface receptors. *Trends Biochem. Sci.* **39**, 447–456 (2014).
38. Dong, X. B., Jiang, Z. H., Peng, Y. L. & Zhang, Z. D. Revealing shared and distinct gene network organization in arabidopsis immune responses by integrative analysis. *Plant Physiol.* **167**, 1186–1203 (2015).
39. Antolin-Llovera, M., Ried, M. K., Binder, A. & Parniske, M. Receptor kinase signaling pathways in plant-microbe interactions. *Annu. Rev. Phytopathol.* **50**, 451–473 (2012).
40. Monaghan, J. & Zipfel, C. Plant pattern recognition receptor complexes at the plasma membrane. *Curr. Opin. Plant Biol.* **15**, 349–357 (2012).
41. Li, J. & Tax, F. E. Receptor-like kinases: key regulators of plant development and defense. *J. Integr. Plant Biol.* **55**, 1184–1187 (2013).
42. Igarashi, D., Tsuda, K. & Katagiri, F. The peptide growth factor, phytoalexin, attenuates pattern-triggered immunity. *Plant J.* **71**, 194–204 (2012).
43. Mosher, S. *et al.* The tyrosine-sulfated peptide receptors PSKR1 and PSY1R modify the immunity of Arabidopsis to biotrophic and necrotrophic pathogens in an antagonistic manner. *Plant J.* **73**, 469–482 (2013).
44. Gao, M. *et al.* Regulation of cell death and innate immunity by two receptor-like kinases in Arabidopsis. *Cell Host Microbe* **6**, 34–44 (2009).
45. Halter, T. *et al.* The leucine-rich repeat receptor kinase BIR2 is a negative regulator of BAK1 in plant immunity. *Curr. Biol.* **24**, 134–143 (2014).
46. Castells, E. & Casacuberta, J. M. Signalling through kinase-defective domains: the prevalence of atypical receptor-like kinases in plants. *J. Exp. Bot.* **58**, 3503–3511 (2007).
47. Reiterer, V., Evers, P. A. & Farhan, H. Day of the dead: pseudokinases and pseudophosphatases in physiology and disease. *Trends Cell Biol.* **24**, 489–505 (2014).
48. Lewis, J. D. *et al.* The Arabidopsis ZED1 pseudokinase is required for ZAR1-mediated immunity induced by the Pseudomonas syringae type III effector HopZ1a. *Proc. Natl Acad. Sci. USA* **110**, 18722–18727 (2013).
49. Nimchuk, Z. L., Tarr, P. T. & Meyerowitz, E. M. An evolutionarily conserved pseudokinase mediates stem cell production in plants. *Plant Cell* **23**, 851–854 (2011).
50. Chevalier, D. *et al.* STRUBBELIG defines a receptor kinase-mediated signaling pathway regulating organ development in Arabidopsis. *Proc. Natl Acad. Sci. USA* **102**, 9074–9079 (2005).
51. Wang, G. *et al.* The decoy substrate of a pathogen effector and a pseudokinase specify pathogen-induced modified-self recognition and immunity in plants. *Cell Host Microbe* **18**, 285–295 (2015).
52. Gee, C. L. *et al.* A phosphorylated pseudokinase complex controls cell wall synthesis in mycobacteria. *Sci. Signal.* **5**, ra7 (2012).
53. Childers, W. S. *et al.* Cell fate regulation governed by a repurposed bacterial histidine kinase. *PLoS Biol.* **12**, e1001979 (2014).
54. Ladwig, F. *et al.* Phytoalexin regulates growth in Arabidopsis through a response module at the plasma membrane that includes CYCLIC NUCLEOTIDE-GATED CHANNEL17, H⁺-ATPase, and BAK1. *Plant Cell* **27**, 1718–1729 (2015).
55. Fuglsang, A. T. *et al.* Receptor kinase-mediated control of primary active proton pumping at the plasma membrane. *Plant J.* **80**, 951–964 (2014).
56. Merchante, C., Alonso, J. M. & Stepanova, A. N. Ethylene signaling: simple ligand, complex regulation. *Curr. Opin. Plant Biol.* **16**, 554–560 (2013).
57. Wulfetange, K. *et al.* The cytokinin receptors of Arabidopsis are located mainly to the endoplasmic reticulum. *Plant Physiol.* **156**, 1808–1818 (2011).
58. Koizumi, N. *et al.* Molecular characterization of two Arabidopsis Ire1 homologs, endoplasmic reticulum-located transmembrane protein kinases. *Plant Physiol.* **127**, 949–962 (2001).
59. Voisin, D. *et al.* Dissection of the complex phenotype in cuticular mutants of Arabidopsis reveals a role of SERRATE as a mediator. *PLoS Genet.* **5**, e1000703 (2009).
60. Allen, E. *et al.* Evolution of microRNA genes by inverted duplication of target gene sequences in Arabidopsis thaliana. *Nat. Genet.* **36**, 1282–1290 (2004).
61. Allen, E., Xie, Z., Gustafson, A. M. & Carrington, J. C. microRNA-directed phasing during trans-acting siRNA biogenesis in plants. *Cell* **121**, 207–221 (2005).
62. Innes, R. W. *et al.* Identification of a disease resistance locus in Arabidopsis that is functionally homologous to the RPG1 locus of soybean. *Plant J.* **4**, 813–820 (1993).
63. Bisgrove, S. R., Simonich, M. T., Smith, N. M., Sattler, A. & Innes, R. W. A disease resistance gene in Arabidopsis with specificity for two different pathogen avirulence genes. *Plant Cell* **6**, 927–933 (1994).
64. Hinsch, M. & Staskawicz, B. Identification of a new Arabidopsis disease resistance locus, RPS4, and cloning of the corresponding avirulence gene, avrRps4, from Pseudomonas syringae pv. pisi. *Mol. Plant Microbe In.* **9**, 55–61 (1996).
65. Yuan, J. & He, S. Y. The Pseudomonas syringae Hrp regulation and secretion system controls the production and secretion of multiple extracellular proteins. *J. Bacteriol.* **178**, 6399–6402 (1996).
66. Schwab, R., Ossowski, S., Riester, M., Warthmann, N. & Weigel, D. Highly specific gene silencing by artificial microRNAs in Arabidopsis. *Plant Cell* **18**, 1121–1133 (2006).
67. Earley, K. W. *et al.* Gateway-compatible vectors for plant functional genomics and proteomics. *Plant J.* **45**, 616–629 (2006).
68. Wang, D., Weaver, N. D., Kesarwani, M. & Dong, X. N. Induction of protein secretory pathway is required for systemic acquired resistance. *Science* **308**, 1036–1040 (2005).
69. Llave, C., Xie, Z. X., Kasschau, K. D. & Carrington, J. C. Cleavage of Scarecrow-like mRNA targets directed by a class of Arabidopsis miRNA. *Science* **297**, 2053–2056 (2002).
70. Caplan, J. L. *et al.* Induced ER chaperones regulate a receptor-like kinase to mediate antiviral innate immune response in plants. *Cell Host Microbe* **6**, 457–469 (2009).

Acknowledgements

We thank David Baulcombe for providing *rdr6-15* mutant seeds; Johnathan Clark for providing *se-1* mutant seeds; and Artur Jarmolowski and Michael Prigge for providing SE-OE lines. H.J., D.N., Y.E.L. and P.C. were supported by grants from the National Institute of Health (R01 GM093008), the National Science Foundation (IOS-1557812) and an AES-CE Award (PPA-7517H) awarded to H.J. G.C. and L.L. were supported by grants from the National Science Foundation (MCB-1054298), and the National Institutes of Health (R01-GM092772) awarded to G.C. C.J. and J.G. were supported by a grant from Joint Research Fund for Overseas, Hong Kong, and Macao Scholars (31228018) awarded to J.G. and H.J.

Author contributions

H.J. conceived the idea and designed the project; D.N., Y.E.L., P.C., L.L., C.J. and K.P. performed the experiments; H.J., D.N., Y.E.L., P.C., J.G. and G.C. analysed and interpreted the data; H.J., Y.E.L. and D.N. wrote the manuscript; all authors read and approved the final manuscript for publication.

Additional information

Supplementary Information accompanies this paper at <http://www.nature.com/naturecommunications>

Competing financial interests: The authors declare no competing financial interests.

Reprints and permission information is available online at <http://npg.nature.com/reprintsandpermissions/>

How to cite this article: Niu, D. *et al.* miRNA863-3p sequentially targets negative immune regulator *ARLPKs* and positive regulator *SERRATE* on bacterial infection. *Nat. Commun.* **7**:11324 doi: 10.1038/ncomms11324 (2016).



This work is licensed under a Creative Commons Attribution 4.0 International License. The images or other third party material in this article are included in the article's Creative Commons license, unless indicated otherwise in the credit line; if the material is not included under the Creative Commons license, users will need to obtain permission from the license holder to reproduce the material. To view a copy of this license, visit <http://creativecommons.org/licenses/by/4.0/>